Extreme Mechanics Letters 4 (2015) 193–198

Contents lists available at ScienceDirect

Extreme Mechanics Letters

journal homepage: www.elsevier.com/locate/eml

Size and curvature regulate pattern selection in the mammalian brain

Silvia Budday [a], Paul Steinmann [a], Alain Goriely [b], Ellen Kuhl [c,*]

[a] Chair of Applied Mechanics, Department of Mechanical Engineering, University of Erlangen/Nuremberg, 91058 Erlangen, Germany

[b] Mathematical Institute, University of Oxford, Oxford OX2 6GG, United Kingdom

[c] Departments of Mechanical Engineering, Bioengineering, and Cardiothoracic Surgery, Stanford University, 496 Lomita Mall, Stanford, CA 94305, USA

ARTICLE INFO

Article history:
Received 22 January 2015
Received in revised form 14 May 2015
Accepted 16 July 2015
Available online 17 July 2015

Keywords:
Soft matter
Living matter
Thin films
Brain mechanics
Cortical folding
Growth
Instabilities

ABSTRACT

Mammalian brains display a wide variety of shapes and surface morphologies. Their characteristically folded surface is closely correlated to neuronal activity and serves as a clinical indicator for physiological and pathological conditions. Yet, the regulators of pattern formation in evolution and development remain poorly understood. Here we show how brain size and curvature affect the folding pattern in the developing mammalian brain. We model cortical folding as the instability problem of a bilayered system subjected to growth-induced compression. Using analytical estimates and continuum models for finite growth, we systematically explore the effects of geometric factors on the evolution of surface shape. We demonstrate that extrinsic geometric features – including brain size, cortical thickness, and cortical curvature – tightly regulate pattern selection: The mammalian brain is extremely soft and even small environmental changes can create extremely large alterations in its surface morphology. Our simulations explain why gyrification increases with brain size and why longer brains tend to fold more longitudinally than radially. Our results suggest that brain folding is driven, at least in part, by extreme mechanics, rather than by phylogeny alone.

1. Motivation

By reason of its convoluted shape, complex connections, and intriguing individuality the brain remains our least understood organ [1]. Most research activities focus on the neuronal activity on the cellular level and ignore fundamental challenges arising from physical effects at the organ scale. One such open challenge is the morphogenesis of the diverse folding pattern in the mammalian brain [2]. The mammalian brain impressively varies in size, shape, and convolutional complexity [3]. Generally, the absolute brain size scales with body size [4]. Our brain's surface area, however, increases disproportionally faster than its volume: larger mammalian brains appear more convoluted than smaller ones as illustrated in Fig. 1. At the functional level, brain folding maximizes the number of processing units in the outer gray matter layer and minimizes the connections between them in the inner white matter core. The degree of folding is often associated with cognitive abilities [5] and intelligence [6,7]. Abnormal brain development also results in severe pathologies associated with neurological disorders including schizophrenia and autism.

As pointed out more than half a century ago by Sir Wilfrid Le Gros Clark, we need to distinguish precisely between genetic factors and mechanical effects to elucidate

* Corresponding author. Tel.: +1 650 450 0855; fax: +1 650 725 1587.
E-mail addresses: silvia.lettau@ltm.uni-erlangen.de (S. Budday), paul.steinmann@ltm.uni-erlangen.de (P. Steinmann), goriely@maths.ox.ac.uk (A. Goriely), ekuhl@stanford.edu (E. Kuhl).
URL: http://biomechanics.stanford.edu (E. Kuhl).

http://dx.doi.org/10.1016/j.eml.2015.07.004
2352-4316/

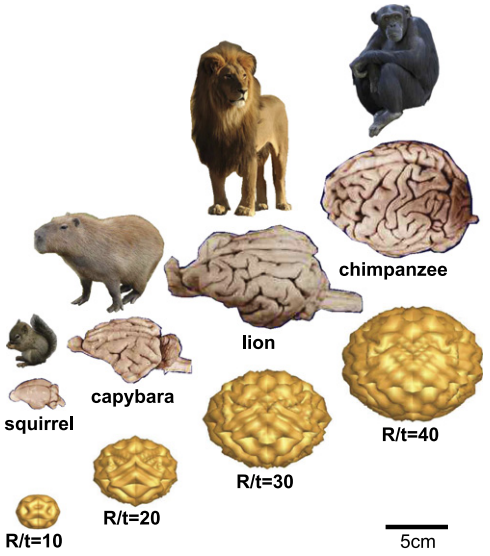

Fig. 1. Mammalian brains vary greatly in size, shape, and gyrification but only marginally in cortical thickness. Simulations of spheroid with growing cortical layer and varying radius-to-thickness ratio predict an increase in gyrification with absolute brain size.

the origin of brain convolutions [8]. To date, hypotheses on how convolutions in the mammalian brain evolve [1,9] and which forces drive the folding process [10,11] remain contradictory. A promising mechanical explanation of brain folding is based on differential growth between the different layers of the brain [12]. During development, the initially smooth outer cortex grows at a faster rate than the inner white matter core [13]. Differential growth gives rise to residual stresses that induce a mechanical instability, which results in surface buckling [14,15]. The stress patterns associated with differential growth theories agree well with physical stress measurements in the developing ferret brain [16]. However, early attempts to model brain folding with differential growth rely on unphysiologically large stiffness ratios between the outer layer and the inner core [10,17]. Recent studies based on the classical instability analyses of a growing bilayered system have revealed correlations between the mode number, the number of folds m_{crit}, the cortical thickness t, and the stiffness ratio between gray and white matter E_g/E_w [13,18],

$$m_{\text{crit}} \propto 1/t \quad \text{and} \quad m_{\text{crit}} \propto \sqrt[3]{E_w/E_g}. \tag{1}$$

However, these relations are only valid in flat cortical layers – which is clearly not the case in the developing brain – and in the linear regime, prior to the onset of folding. A recent study elegantly illustrates the importance of curvature in pattern selection of thin elastic rots deployed on a moving substrate [19]. Here we explore size and curvature effects on pattern selection for a growing elastic layer on an elastic substrate.

2. Analytical model of growing bi-layered system

To understand the role of curvature, we first consider the simple morpholelastic beam model [20] illustrated in Fig. 2.

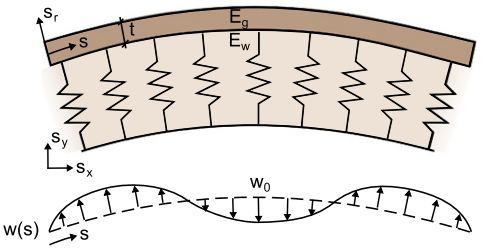

Fig. 2. Growing cortical layer on a curved elastic substrate.

We characterize the deformation of the beam through the stretch $\lambda = s' \equiv \partial s/\partial S$, the partial derivative of the arc length of the grown beam $s(S,t)$ with respect to the arc length of the initial, ungrown beam S, where $\{\circ\}' = \mathrm{d}\{\circ\}/\mathrm{d}S$ denotes the derivative with respect to the initial arc length S. We decompose this total stretch into an elastic stretch λ^e and a growth stretch λ^g [21],

$$\lambda = \lambda^e \lambda^g = \frac{\partial s}{\partial S}. \tag{2}$$

We further introduce the Cartesian coordinate system $\{\boldsymbol{e}_x, \boldsymbol{e}_y\}$ and the angle θ between the horizontal direction $\boldsymbol{e}_x$ and the centerline of the beam. The equilibrium equations of a stretchable but unshearable morphoelastic beam in the plane are

$$\begin{aligned} &n_x' + f_x = 0 \quad \text{and} \quad n_y' + f_y = 0 \\ &EI\,\theta'' + \lambda^e \lambda^{g2}[n_y \cos\theta - n_x \sin\theta] = 0, \end{aligned} \tag{3}$$

where $\boldsymbol{n} = n_x \boldsymbol{e}_x + n_y \boldsymbol{e}_y$ is the resultant force, $\boldsymbol{f} = f_x \boldsymbol{e}_x + f_y \boldsymbol{e}_y$ is the external force per unit initial length, and $EI = E_g b\, t^3/12$ is the bending stiffness of a beam of width b and thickness t [20]. We adopt a linear constitutive law to correlate axial stress $[n_x \cos\theta + n_y \sin\theta]/A$ and axial strain $\varepsilon = \lambda^e - 1$ as

$$n_x \cos\theta + n_y \sin\theta = EA[\lambda^e - 1], \tag{4}$$

where $EA = E_g b\, t$ is the axial stiffness of the beam. The effect of the foundation is subtle to model and subject to many studies [22]. Here, we first consider the trivial equilibrium by assuming that both the foundation and the beam deform circularly with radii R and $r^{(0)}$. In polar coordinates $\{\boldsymbol{e}_r, \boldsymbol{e}_\varphi\}$, the external force from the foundation to the beam is $f_r^{(0)} = -E_w b[r^{(0)}/R - 1]$. The trivial solution is then $r^{(0)} = R\,[1 + \lambda^e \lambda^g]$ and $\varphi^{(0)} = S/R$, with $n^{(0)} \equiv N = E_g b\, t\,[1/\lambda^g - 1]$ and

$$\lambda^e = \frac{E_g t + E_w R}{E_g t + E_w R\,\lambda^g} = \frac{1}{\lambda^g} + \lambda_1^e \kappa + \mathcal{O}(\kappa^2), \tag{5}$$

where $\kappa = 1/R$ is the initial curvature and $\lambda_1^e = E_g t(\lambda^g - 1)/(E_w \lambda^{g2})$. As expected, we observe that the radius of the beam increases with growth. We can now consider small deviations ϵ around this trivial solution for small κ by considering the expansions $r(S) = r^{(0)} + \epsilon\, w(S)$ and $f_r = f_r^{(0)} + \epsilon\, q$ and by further expanding all variables in powers of κ. After simplification, this double expansion leads to the fourth-order beam equation for the deflection

w,

$$EI\,w'''' + N\lambda^{g} w'' - \lambda^{g} q + \kappa\lambda^{g}\lambda_1^{e}[EI\,w'''' + EA[2\lambda^{g} - 3]w'' - 3\lambda^{g} q] = 0. \quad (6)$$

This equation has a number of interesting features: In the absence of growth, $\lambda^{g} = 1$, for an inextensible beam, $\lambda^{e} = 1$, it simplifies to the classical equation $EI\,w'''' + N\,w'' - q = 0$ for a beam under a compressive force N on a foundation [22]. For a flat foundation, $\kappa = 0$, it generalizes the engineering beam equation to the equation of a growing morphoelastic beam [23]. Curvature increases the effective bending stiffness by a factor $[1 + \kappa\,\lambda^{g}\lambda_1^{e}]$, while reducing the effective load and increasing the foundation stiffness. We thus expect curvature to delay instabilities: in a domain of regionally varying curvature, folding should emerge first in regions of low curvature. Let us now characterize the growth of the beam by the growth parameter $\vartheta = \lambda^{g}$. We can then calculate the critical amount of growth ϑ^{crit} at which the instability occurs using a Fourier analysis of Eq. (6) with mth mode $w = w_0 \cos(mS/t)$. The corresponding reaction force of the foundation, $q = -E_{\text{w}} b\, m\, w_0/(2t)$, has been found by Biot as the solution of an elastic half-space [22]. A similar solution for a finite foundation of depth R provides a correction term proportional to $\exp(-mR/t)$, which is beyond all orders in the curvature and shall be ignored. The mth mode is a solution provided that the mode number m satisfies a dispersion relation,

$$\begin{aligned}\Delta(\vartheta, m) = {} & E_{\text{w}}\vartheta[12E_{\text{g}}m + E_{\text{g}}m^3 \\ & + 6E_{\text{w}}\vartheta - 12E_{\text{g}}m\vartheta] \\ & + \kappa E_{\text{g}} t[\vartheta - 1][36E_{\text{g}}m + E_{\text{g}}m^3 \\ & + 18E_{\text{w}}\vartheta - 24E_{\text{g}}m\vartheta].\end{aligned}$$

By simultaneously solving $\Delta(\vartheta, m) \doteq 0$ and $\partial_m \Delta(\vartheta, m) \doteq 0$, we can determine the critical growth ϑ^{crit} and the critical mode number m^{crit}. We expand the solution to order κ as $\vartheta^{\text{crit}} = \vartheta_0 + \kappa\vartheta_1$ and $m^{\text{crit}} = m_0 + \kappa m_1$, where m_0 is the first positive root of $4E_{\text{g}}m_0^3 - 3E_{\text{w}}[4 + m_0^2] = 0$, and $\vartheta_0 = 1/4\,[4 + m_0^2]$, from which we recover the scaling in Eq. (1). To first order, the curvature correction is

$$\vartheta_1 = \frac{E_{\text{g}} t\, m_0^2[2E_{\text{g}}m_0[5m_0^2 - 12] - 9E_{\text{w}}[m_0^2 + 4]]}{8\,E_{\text{w}}[3E_{\text{w}}[m_0^2 + 4] - E_{\text{g}}m_0[5m_0^2 + 12]]},$$

$$m_1 = \frac{E_{\text{g}} t\, m_0[32E_{\text{g}}m_0^3 - 3E_{\text{w}}[m_0^4 + 24m_0^2 + 80]]}{4E_{\text{w}}[m_0^2 + 4][3E_{\text{w}}[m_0^2 + 4] - E_{\text{g}}m_0[5m_0^2 + 12]]}.$$

As an example, for a stiffness ratio of $E_{\text{g}}/E_{\text{w}} = 3$ between beam and foundation, the critical growth and mode number are $\vartheta^{\text{crit}} \approx 1.3 + 0.9\,\kappa\, t$ and $m^{\text{crit}} \approx 1.09 + 0.75\,\kappa\, t$. This estimate indicates that curvature has a delaying effect on the onset of the instability.

3. Continuum model of growing bi-layered system

In light of the previous remarks, we expand the model problem of the curved beam to a fully three-dimensional, nonlinear continuum model [24]. We characterize local kinematic changes through the deformation gradient $\boldsymbol{F} = \partial\boldsymbol{x}/\partial\boldsymbol{X}$, the partial derivative of points in the grown configuration $\boldsymbol{x}$ with respect to their initial position in the ungrown reference configuration $\boldsymbol{X}$. By analogy to Eq. (2), we adopt the classical multiplicative decomposition of the deformation gradient into an elastic part $\boldsymbol{F}^{\text{e}}$ and a growth part $\boldsymbol{F}^{\text{g}}$ [25,26],

$$\boldsymbol{F} = \boldsymbol{F}^{\text{e}} \cdot \boldsymbol{F}^{\text{g}} = \partial\boldsymbol{x}/\partial\boldsymbol{X}. \quad (7)$$

During brain development, neural progenitor cell division, neuronal migration, and the formation of neural connections cause an excessive tangential expansion of the cortical layer [27]. We model these biological processes through a single scalar-valued variable, the tangential gray matter area growth ϑ_{g},

$$\boldsymbol{F}^{\text{g}} = \vartheta_{\text{g}}^{1/2}\boldsymbol{I} + [1 - \vartheta_{\text{g}}^{1/2}]\,\boldsymbol{n}\otimes\boldsymbol{n} \quad \text{with } \dot{\vartheta}_{\text{g}} = G_{\text{g}}. \quad (8)$$

Here, $\boldsymbol{I}$ is the second order unit tensor, $\boldsymbol{n}$ is the initial outward pointing cortical normal, and G_{g} is the cortical expansion rate. The gray matter elastic tensor then follows as $\boldsymbol{F}^{\text{e}} = [\boldsymbol{F} + [\vartheta_{\text{g}}^{1/2} - 1]\boldsymbol{F}\cdot\boldsymbol{n}\otimes\boldsymbol{n}]/\vartheta_{\text{g}}^{1/2}$. As the outer layer grows, it pulls on the underlying inner core, and activates volumetric white matter growth ϑ_{w},

$$\boldsymbol{F}^{\text{g}} = \vartheta_{\text{w}}^{1/3}\boldsymbol{I} \quad \text{with } \dot{\vartheta}_{\text{w}} = G_{\text{w}}[J^{\text{e}} - 1]. \quad (9)$$

The axon elongation rate G_{w} reflects the ability of axons to chronically increase their length when stretched beyond their physiological limit, $J^{\text{e}} = \det(\boldsymbol{F}^{\text{e}}) > 1$ [28]. The white matter elastic tensor then follows as $\boldsymbol{F}^{\text{e}} = \boldsymbol{F}/\vartheta_{\text{w}}^{1/3}$. We assume that only the elastic deformation generates stress and model gray and white matter as nonlinear hyperelastic Neo-Hookean materials with an elastic energy density $\psi = \frac{1}{2}\lambda\,\ln^2(J^{\text{e}}) + \frac{1}{2}\mu\,[\boldsymbol{F}^{\text{e}} : \boldsymbol{F}^{\text{e}} - 3 - 2\,\ln(J^{\text{e}})]$, where λ and μ are the Lamé constants. The Piola stress follows as the partial derivative of the energy density ψ with respect to the deformation gradient $\boldsymbol{F}$,

$$\boldsymbol{P} = \partial\psi/\partial\boldsymbol{F} = [\mu\,\boldsymbol{F}^{\text{e}} + [\lambda\,\ln(J^{\text{e}}) - \mu]\,\boldsymbol{F}^{\text{e}-\text{t}}]\cdot\boldsymbol{F}^{\text{g}-\text{t}}. \quad (10)$$

On the time scale of brain development – in humans on the order months – growth is a quasi-static process. This implies that the balance of linear momentum reduces to the vanishing divergence of the Piola stress,

$$\text{Div}(\boldsymbol{P}) \doteq \boldsymbol{0}. \quad (11)$$

The balance of linear momentum (11) together with the kinematics of finite growth (7), the constitutive equation (10), and the growth kinematics and kinetics for gray matter (8) and white matter (9) provide the set of governing equations for brain development. To explore the nonlinear dynamics of pattern selection, we discretize the set of equations using finite elements and solve it incrementally iteratively using a Newton–Raphson scheme implemented in MATLAB. We model the developing brain as an excessively growing outer gray matter layer of thickness t confined by an ellipsoidal inner white matter core of semi-axes R_{x}, R_{y}, and R_{z}. We discretize one eighth of the ellipsoid with 4600 tri-linear Q1 elements, 5303 nodes, 15,909 degrees of freedom to represent the deformation, and 36,800 integration points to represent growth. We assume axisymmetry in all three planes. With 80 elements along the circumference, this is the finest discretization that still runs

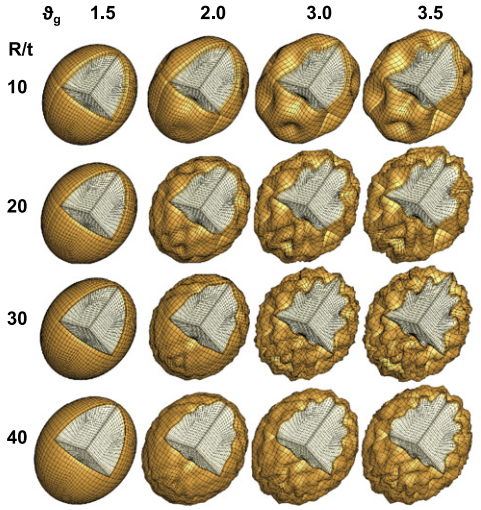

Fig. 3. Emerging folding patterns of a growing shell on a spheroidal substrate for varying radius-to-thickness ratios R/t. Folding emerges first in regions of lowest curvature. Increasing the ratio R/t enhances folding.

Table 1
Emerging number of folds m in xy-, xz-, and yz-planes for varying radius-to-thickness ratios R/t.

R/t	m_{xy}	m_{xz}	m_{yz}
10	6	8	6
20	10	10	8
30	12	12	12
40	14	16	14

on a single laptop computer, and yet captures the folding pattern with five to 15 elements per wavelength. We assume elastic parameters of $\mu_w = 3$ kPa and $\lambda_w = 33$ kPa, an elastic stiffness ratio of $E_g/E_w = 3$ and a growth ratio of $G_g/G_w = 1/10$ [29].

4. Results

Fig. 3 illustrates the emerging pattern formation of a growing shell on a spheroidal substrate for varying radius-to-thickness ratios R/t at fixed semi-axes $R_x = R_y = R$ and $R_z = 1.2R$. The unequal semi-axes imply an inhomogeneous curvature and induce nonuniform stresses in the outer layer [30]. In agreement with the analytical prediction in Eq. (6), the instability emerges first in the equatorial region of lowest curvature [31] (see Appendix A). For example, for $R/t = 30$, the numerical critical growth value of $\vartheta^{crit} \approx 1.34$ is in good agreement with the analytical estimate of $\vartheta^{crit} \approx 1.3 + 0.9\,\kappa t = 1.33$.

Table 1 summarizes the number of folds m in the xy-, xz-, and yz-planes. As an inherent limitation of our axisymmetric model, all our fold numbers are limited to even numbers. In agreement with the literature [32,33], we observe that the fold number increases with increasing radius-to-thickness ratio R/t: on a flat substrate, our analytical model indicates that the number of folds increases linearly with (R/t); on a spheroidal substrate, our computational model suggests that the mode number increases roughly proportional to $(R/t)^{5/8}$. This value is lower than

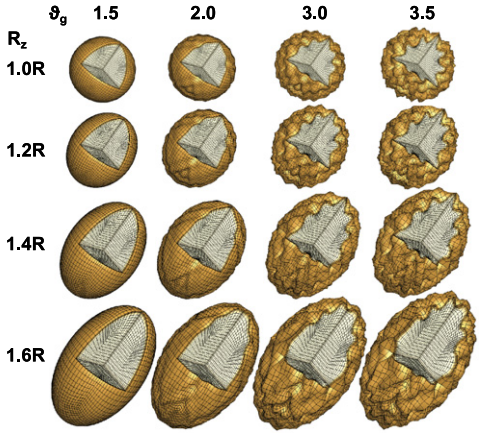

Fig. 4. Emerging folding patterns of a growing shell on a spheroidal substrate for varying spheroid lengths R_z at fixed radius-to-thickness ratio $R/t = 30$. Folding emerges first in regions of lowest curvature. Increasing the lengths R_z triggers longitudinal folding.

(R/t) and $(R/t)^{3/4}$, the values reported for less curved flat and cylindrical substrates [34]. This scaling is consistent with qualitative observations in the developing brain of preterm infants where folding occurs first in the forebrain [35]. With progressive growth, the initial folding pattern eventually undergoes secondary bifurcations and transforms into increasingly complex morphologies [31] (see Appendix A). These observations are in good agreement with studies of mammalian brains, which reveal that gyrification increases with brain size, while the cortical thickness remains relatively well preserved across different species [3,8]. Taken together, the results in Fig. 3 explain why the surface-to-volume ratio of the mammalian brain increases disproportionally with brain size and why larger brains tend to be more convoluted—independent of phylogenetic effects [3].

Fig. 4 demonstrates how the variation of the third semi-axis R_z affects the folding pattern: A progressive increase of the long-axis radius R_z favors the emergence of longitudinal folds [31] (see Appendix A). These results are consistent with anatomical observations in mammalian brains: Narrow elongated brains fold predominantly in the longitudinal direction, while broader and rounder brains tend to fold in the transverse direction [8].

Fig. 5 supports these observations: Transverse folding dominates in the brachycephalic wombat brain, whereas longitudinal folding dominates in the dolichocephalic hyrax brain. These findings agree with cortical folding in the mammalian brain, were transverse folding dominates in the brachycephalic Chinese skull, whereas longitudinal folding predominates in the dolichocephalic Dutch skull [36].

Fig. 6 illustrates how a simple variation from a spheroidal core to a triaxial ellipsoid further enhances the variety of three-dimensional self-assembled folding morphologies for a gray matter area growth of $\vartheta_g = 3.5$. While the critical wavenumber m_{crit} in the equatorial plane of a spheroid with equal semi-axes $R_x = R_y = R$ is independent of the third semi-axis R_z, left column, m_{crit} varies with varying R_z in general triaxial ellipsoids with three unequal

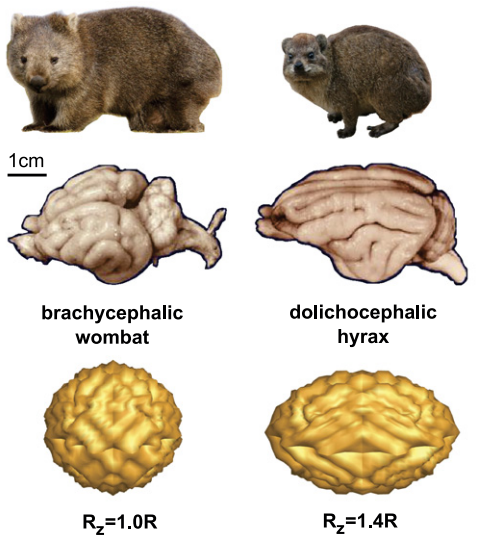

Fig. 5. Mammalian brains vary greatly in ellipticity and gyrification. Simulations of spheroid with growing cortical layer and varying ellipticity predict transverse folding in the brachycephalic skull and longitudinal folding in the dolichocephalic skull.

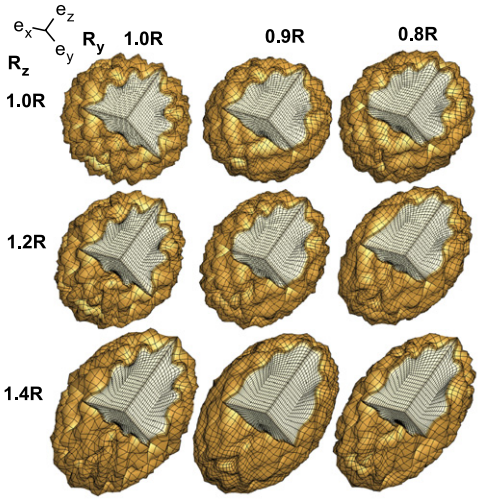

Fig. 6. Folding patterns of a growing shell on an ellipsoidal substrate for varying semi-axes $R_x = R$, R_y and R_z at fixed radius-to-thickness ratio $R/t = 30$ and $\vartheta_g = 3.5$.

semi-axes, middle and right column. This trend suggests that gyrification is highly regulated by the variability of brain shape. Considering the relatively simple geometrical effects studied in this letter, the excessive complexity and inhomogeneity of the mammalian brain is likely to generate exceedingly more complex morphological patterns just by its mere shape.

While our computational model predicts conceptually reasonable surface morphologies that agree well with analytical estimates, our simulations have a few limitations: First, our current model does not include the influence of the skull, which has previously been demonstrated to flatten out the individual gyri and sulci [17], but not affect the gyral wavelength, which was the major focus of the current study. Second, our current discretization with 15,909 displacement degrees of freedom and 36,800 internal variables for growth is relatively coarse and would need to be refined to simulate larger radius-to-thickness ratios with smaller wavelengths [37]. With more computational power, we could also release the symmetry conditions to capture odd fold numbers. Third, and most importantly, unfortunately, we know very little about the stiffness ratio between gray and white matter [17], a parameter whose third root is directly proportional to the gyral wavelength [13]. While the *ex vivo* stiffness ratio of the mature, myelinated brain is on the order of one [38], the *in utero* stiffness ratio of the immature, unmyelinated brain remains unknown. To address this limitation, we are currently performing nanoindentation experiments at different time points to quantify stiffness changes during brain development. Here, we have postulated that at the onset of folding, unmyelinated white matter is softer than gray matter. For reversed stiffness ratios, we did observe highly oscillatory, unphysiologic folding patterns [39].

5. Concluding remarks

The objective of this study was to investigate the morphogenesis of the developing mammalian brain using simplified models of differential growth in curved geometries. Our study provides quantitative estimates for the onset of folding and pattern formation: in a homogeneous system, curvature has a delaying effect on the formation of instabilities; in a heterogeneous system, instabilities occur first in regions of lowest curvature. With progressive growth beyond the initial instability, the surface undergoes secondary bifurcations in the nonlinear regime and forms intricate morphologies. Our models explain why mammalian brains with a similar cortical thickness but a different size naturally display a disproportional increase in surface area with increasing brain volume. They also explain why elongated brains tend to develop longitudinal folds while rounded brains are more uniformly folded. Understanding the interplay between geometry, mechanics, and morphogenesis can help distinguish mechanical factors during evolution and neurodevelopment from phylogenetic effects. This approach provides insight into brain form and, ultimately, brain function using the fundamental laws of physics.

Acknowledgments

We acknowledge support through the German National Science Foundation grant STE 544/50-1, the Wolfson/Royal Society Merit Award Reintegration Grant under EC Framework VII, the Stanford Bio-X Interdisciplinary Initiatives Program, and the National Institutes of Health grant U01 HL119578.

Appendix A. Supplementary data

Supplementary material related to this article can be found online at http://dx.doi.org/10.1016/j.eml.2015.07.004.

References

[1] R. Willemet, Understanding the evolution of mammalian brain structures; the need for a (new) cerebrotype approach, Brain Sci. 2 (2012) 203–224.
[2] A. Goriely, M.G.D. Geers, G.A. Holzapfel, J. Jayamohan, A. Jerusalem, S. Sivaloganathan, W. Squier, J.A.W. van Dommelen, S. Waters, E. Kuhl, Mechanics of the brain: Perspectives, challenges, and opportunities, Biomech. Model. Mechanobiol. (2015) http://dx.doi.org/10.1007/s10237-015-0662-4.
[3] W. Welker, Cerebral Cortex, Springer, 1990.
[4] W. Welker, I.J. Johnson, A. Noe, Comparative mammalian brain collections. http://brainmuseum.org.
[5] S. Herculano-Houzel, The human brain in numbers: a linearly scaled-up primate brain, Front. Hum. Neurosci. 3 (2009) 31.1–31.11.
[6] M.C. Diamond, A.B. Scheibel, G.M. Murphy Jr., T. Harvey, On the brain of a scientist: Albert Einstein, Exp. Nephrol. 88 (1985) 198–204.
[7] E. Luders, K.L. Narr, R.M. Bilder, P.R. Szeszko, M.N. Gurbani, L. Hamilton, A.W. Toga, C. Gaser, Mapping the relationship between cortical convolution and intelligence: effects of gender, Cereb. Cortex 18 (2008) 2019–2026.
[8] W. Le Gros Clark, Essays on Growth and Form, Oxford University Press, London, 1945.
[9] B.L. Finlay, R.B. Darlington, Linked regularities in the development and evolution of mammalian brains, Science 268 (1995) 1578–1584.
[10] D.P. Richman, R.M. Stewart, J.W. Hutchinson, V.S. Caviness, Mechanical model of brain convolutional development, Science 189 (1975) 18–21.
[11] D.C. Van Essen, A tension-based theory of morphogenesis and compact wiring in the central nervous system, Nature 385 (1997) 313–318.
[12] L. Jin, S. Cai, Z. Suo, Creases in soft tissues generated by growth, EPL Front. Phys. 95 (2011) 64002.1–64002.6.
[13] P.V. Bayly, R. Okamoto, G. Xu, Y. Shi, L.A. Taber, A cortical folding model in- corporating stress-dependent growth explains gyral wavelengths and stress patterns in the developing brain, Phys. Biol. 10 (2013) 016005.
[14] P. Ciarletta, V. Balbi, E. Kuhl, Pattern selection in growing tubular tissues, Phys. Rev. Lett. 113 (2014) 248101.
[15] M. Taylor, K. Bertoldi, D.J. Steigmann, Spatial resolution of wrinkle patterns in elastic sheets at finite strain, J. Mech. Phys. Solids 62 (2014) 163–180.
[16] I.H. Smart, G.M. McSherry, Gyrus formation in the cerebral cortex in the ferret. I. Description of the external changes, J. Anat. 146 (1986) 141–152.
[17] T. Tallinen, J.Y. Chung, J.S. Bigginsand, L. Mahadevan, Gyrification from constrained cortical expansion, Proc. Natl. Acad. Sci. 111 (2014) 12667.
[18] S. Budday, C. Raybaud, E. Kuhl, A mechanical model predicts morphological abnormalities in the developing human brain, Sci. Rep. 4 (2014) 5644.
[19] K. Jawed, P.M. Reis, Pattern morphology in the elastic sewing machine, Extrem. Mech. Lett. 1 (2014) 76–82.
[20] D.E. Moulton, T. Lessinnes, A. Goriely, Morphoelastic rods Part 1: A single growing elastic rod, J. Mech. Phys. Solids 61 (2013) 398–427.
[21] E.K. Rodriguez, A. Hoger, A.D. McCulloch, Stress-dependent finite growth in soft elastic tissues, J. Biomech. 27 (1994) 455–467.
[22] M.A. Biot, Bending of an infinite beam on an elastic foundation, ZAMM Z. Angew. Math. Mech. 2 (1922) 165–184.
[23] S. Budday, P. Steinmann, E. Kuhl, The role of mechanics during brain development, J. Mech. Phys. Solids 72 (2014) 75–92.
[24] D.J. Steigmann, R.W. Ogden, Classical plate buckling theory as the small-thickness limit of three-dimensional incremental elasticity, ZAMM Z. Angew. Math. Mech. 94 (2014) 7–20.
[25] A. Goriely, M. BenAmar, Differential growth and instability in elastic shells, Phys. Rev. Lett. 94 (2005) 198103.
[26] K. Garikipati, The kinematics of biological growth, Appl. Mech. Rev. 62 (2009) 030801.
[27] T. Sun, R.F. Hevner, Growth and folding of the mammalian cerebral cortex: from molecules to malformations, Nat. Rev. Neurosci. 15 (2014) 217–232.
[28] D. Bray, Axonal growth in response to experimentally applied mechanical tension, Dev. Biol. 102 (1984) 379–389.
[29] M. Holland, K.E. Miller, E. Kuhl, Emerging brain morphologies from axonal elongation, Ann. Biomed. Eng. 43 (2015) 1640–1653.
[30] R. Marcombe, S. Cai, W. Hong, X. Zhao, Y. Lapusta, Z. Suo, A theory of constrained swelling of a pH-sensitive hydrogel, Soft Matter 6 (2010) 784–793.
[31] See supplemental movies S1, S2, and S3 for the emergence of pattern formation on different geometries.
[32] P. Ciarletta, Buckling instabilities in growing tumor spheroids, Phys. Rev. Lett. 110 (2013) 158102.
[33] B. Li, F. Jia, Y.-P. Cao, X.-Q. Feng, H. Gao, Surface wrinkling patterns on a core–shell soft sphere, Phys. Rev. Lett. 106 (2011) 234301.
[34] J. Yin, Z. Cao, C. Li, I. Sheinman, X. Chen, Stress-driven buckling patterns in spheroidal core/shell structures, Proc. Natl. Acad. Sci. 105 (2008) 19132–19135.
[35] C. Raybaud, T. Ahmad, N. Rastegar, M. Shroff, M. Al Nassar, The premature brain: developmental and lesional anatomy, Neurorad 55 (2013) 23–40.
[36] A.J. van Bork-Feltkamp, Uitkomsten van een Onderzoek van een 60-tal Hersenen van Chineezen, Versluy, Amsterdam, 1930.
[37] T. Tallinen, J.S. Biggins, L. Mahadevan, Surface sulu in squeezed soft solids, Phys. Rev. Lett. 110 (2013) 024302.
[38] S. Budday, R. Nay, R. de Rooij, P. Steinmann, T. Wyrobek, T.C. Ovaert, E. Kuhl, Mechanical properties of gray and white matter brain tissue by indentation, J. Mech. Behav. Biomed. Mater. 46 (2015) 318–330.
[39] S. Budday, E. Kuhl, J.W. Hutchinson, Period-doubling and period-tripling in growing bilayered systems, Phil. Mag. (2015) http://dx.doi.org/10.1080/14786435.2015.1014443.